Atlases of Cardiac Fiber Differential Geometry

Emmanuel Piuze[1], Herve Lombaert[1], Jon Sporring[1,2], Gustav J. Strijkers[3], Adrianus J. Bakermans[3], and Kaleem Siddiqi[1]

[1] School of Computer Science & Centre for Intelligent Machines, McGill University
[2] eScience Center, Department of Computer Science, University of Copenhagen
[3] Department of Biomedical Engineering, Eindhoven University of Technology

Abstract. Studies of intra-species cardiac fiber variability tend to focus on first-order measures such as local fiber orientation. Recent work has shown that myofibers bundle locally into a particular type of minimal surface, the generalized helicoid model (GHM), which is described by three biologically meaningful curvature parameters. In order to allow intra-species comparisons, a typical strategy is to divide the parameters of the generalized helicoid by heart diameter. This normalization does not compensate for variability in myocardial shape between subjects and makes interpretation of intra-species results difficult. This paper proposes to use an atlas of rat and dog myocardium, obtained using diffeomorphic groupwise Log-demons, to register all hearts in a common reference shape to perform the normalization. In this common space the GHM is estimated for all hearts and compared using an improved fitting method. Our results demonstrate improved consistency between GHM curvatures within a species and support a direct relation between myocardial shape and fiber curvature in the heart.

1 Introduction

The study of heart structure and function is essential for the diagnosis and treatment of cardiac diseases, which are the leading cause of death in the world. The analysis of cardiac fiber structure is of particular interest [1] since it plays a key role in the mechanical function, electrophysiology and remodeling processes of the heart [2]. The understanding of the complex organization of cardiac fibers has traditionally been based on histological studies [3], but recent advances in diffusion tensor imaging (DT-MRI) has opened the possibility to look at intact tissue in three dimensions [4, 5]. Various species [6–8] have been studied under DT-MRI and statistical atlases have been built for human [9] and canine [10] hearts. These studies have focused largely on the orientation of individual myofibers [11]. Recently, Savadjiev *et al.* have shown that across mammalian species, heart wall fibers bundle locally into a special minimal surface, the generalized helicoid [12].

The Generalized Helicoid Model (GHM) allows one to locally characterize second-order properties of fiber orientation via three curvature parameters, K_T, K_N and K_B. The direct relation between these parameters and the theory of moving frames in differential geometry was recently studied in [13] and their

S. Ourselin, D. Rueckert, and N. Smith (Eds.): FIMH 2013, LNCS 7945, pp. 442–449, 2013.

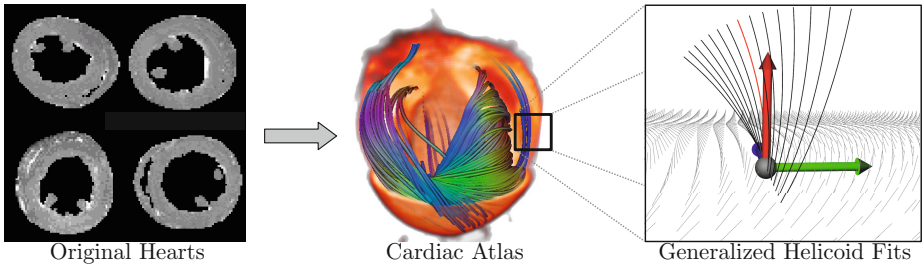

Fig. 1. 1) From an original set of DTI images (4 rat hearts are shown), an atlas of cardiac fibers is constructed via a registration process and 2) At each location in the atlas a GHM is fit to each subject's fiber orientation field. This permits a statistical analysis of the parameters $K_{T,N,B}$ for the species

generative capabilities were evaluated in [14]. In the context of cardiac fiber modeling, the curvature parameters describe bending along the direction of a fiber (K_T), spreading across fibers lying parallel to the heart wall (K_N) and the turning of fibers within a transmural penetration from epicardium to endocardium (K_B). The magnitude of these parameters depend on the underlying scale at which they are computed and must therefore be adjusted in order to make comparisons between subjects. In [12,13], the parameters were normalized by a factor corresponding to the left ventricular diameter. However, this normalization strategy does not compensate for local variability in myocardial shape between subjects.

In this paper we propose a species-specific atlas of myocardial variation to permit inter-subject comparisons (see Fig. 1) where: 1) The shape of each heart is warped using diffeomorphic groupwise Log demons [15] to a common reference shape, 2) the local fiber direction is transported following this deformation to the atlas and 3) GHMs are fit to the warped DTI volumes via a continuous optimization method. These steps are described in Section 2 and results for rat and canine datasets are shown in Section 3.

2 Methods

The total transmural change in fiber orientation is about 110° from epicardium to endocardium for many mammalian species [16]. The GHM measures the change in this orientation per unit step size along particular directions and thus depends on heart wall shape and thickness. In order to compensate for these shape differences, the B_0 image of each heart, which is acquired in the absence of diffusion gradients, is registered to a species-specific atlas [9]. The framework described in this article is consequently based on a registration of the B_0 images for aligning the diffusion orientations. The GHM parameters of fit can then be compared across different subjects using this common reference shape. The operations involved in the registration and fitting procedures are discussed next.

2.1 Atlas Construction Using Groupwise Log-Demons

In order to handle large variations in right ventricle collapse in the datasets, the diffeomorphic groupwise Log-Demons method [15] was used for registration since it can better handle large tissue deformations. The B_0 volume is first segmented for all N hearts by thresholding the background and residuals such as fat and blood around the myocardium. The resulting images $I_{1\ldots N}$ are then transformed to an average heart $\tilde{I}$ of the corresponding species. The respective transformations $\phi_{I_i \mapsto \tilde{I}}$ from the initial images I_i to the average image $\tilde{I}$ are computed in a joint framework using diffeomorphic groupwise Log-demons. This registration minimizes an energy $E = \frac{1}{N}\sum_{i=1}^{N}\left(\mathrm{Sim}(\tilde{I}, I_i \circ \phi_i) + \lambda \mathrm{Reg}(\phi_i)\right)$, where $\mathrm{Sim}(\tilde{I}, I_i')$ is a similarity term and where $\mathrm{Reg}(\phi)$ is a regularization term.

The transformations $\phi_{1\ldots N}$ allow the warping of the tensor fields $D_{1\ldots N}$ of all hearts onto a common reference shape. The atlas of cardiac fibers is obtained as the set of diffusion tensor fields warped onto the average shape of all hearts. GHMs can then be fit to the fiber orientation data in the warped hearts.

2.2 Fitting the Generalized Helicoid Model

The generalized helicoid model was introduced in [12] to capture fiber orientation within a volumetric neighborhood in the heart wall. At a voxel position $\boldsymbol{x}_0$, the model is expressed in a local orthonormal coordinate system $\boldsymbol{x} = \alpha \boldsymbol{T}(\boldsymbol{x}_0) + \beta \boldsymbol{B}(\boldsymbol{x}_0) + \gamma \boldsymbol{N}(\boldsymbol{x}_0)$, where $\boldsymbol{T}$ is the fiber direction measured using DT-MRI, $\boldsymbol{B}$ is the orthogonal component to $\boldsymbol{T}$ of the gradient of the shortest distance to epicardium, and $\boldsymbol{N} = \boldsymbol{B} \times \boldsymbol{T}$. The GHM generates a local field of directions $\boldsymbol{v}(\boldsymbol{x}, \boldsymbol{K}) = \boldsymbol{T}\cos\theta + \boldsymbol{N}\sin\theta$, where the orientation function θ is given by

$$\theta(\alpha, \beta, \gamma) = \arctan\left(\frac{K_T\alpha + K_N\gamma}{1 + K_N\alpha - K_T\gamma}\right) + K_B\beta, \tag{1}$$

and where $\boldsymbol{K} = (K_T, K_N, K_B)$ are parameters of the GHM. The local plane spanned by $\boldsymbol{T}$ and $\boldsymbol{N}$ is referred to as the *tangent plane*. K_T describes the bending of a fiber along its direction in this tangent plane, K_N describes the spreading of fibers along a direction in the tangent plane normal to the fiber direction, and K_B describes the rotation of fibers projected onto the local heart wall from epicardium to endocardium or equivalently a variation of the helix angle. Fig. 1 shows a GHM orientation field generated with helicoid parameters $\boldsymbol{K} = (-0.5, 0, -0.3)$.

In contrast with previous work, where the GHM parameter vector $\boldsymbol{K}$ was estimated in coarse discrete bins using relaxation labeling methods [12], a continuous approach using a Nelder-Mead optimization scheme is used. This allows for more precise measures of parameter values. The optimization problem selects the parameters $\boldsymbol{K}$ that minimize the average angular difference between the measured and predicted directions in isotropic neighborhoods $\mathcal{N}(\boldsymbol{x}_0)$ where $|\mathcal{N}_i| = i^3$ for odd $i \in \mathbb{Z}$,

$$\boldsymbol{K} = \arg\min_{\boldsymbol{K}} \frac{1}{|\mathcal{N}|} \sum_{\boldsymbol{x} \in \mathcal{N}(\boldsymbol{x}_0)} \arccos\left(\boldsymbol{T}(\boldsymbol{x}) \cdot \frac{\boldsymbol{v}(\boldsymbol{x}, \boldsymbol{K})}{||\boldsymbol{v}(\boldsymbol{x}, \boldsymbol{K})||_2} \right) + \lambda ||\boldsymbol{K}||_2^2, \qquad (2)$$

and where λ is a regularization term that penalizes high curvature values.

3 Results

Atlases and GHM fits were constructed using two datasets of healthy *ex vivo* hearts that consist of 8 rats (size $64^2 \times 128$, resolution 0.25^3 mm^3) and 8 dogs (size $300^2 \times 333$, resolution 0.3125^3 mm^3, [6]). The registration is evaluated by measuring the angular difference at each voxel between all hearts and the average heart. The mode of the distribution is of 9.5° for rats (Fig. 2) and 6.8° for dogs. These angular differences are smaller than the reported angular difference of 10.1° for dogs in [10] and of 13.3° for humans in [17]. The effect of registration on the GHM parameters is evaluated next.

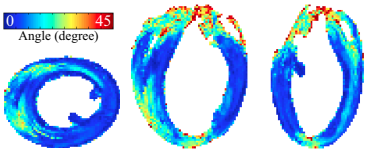

Fig. 2. Angular variation of fiber directions in the atlas of 8 rats

3.1 Effect of Registration on GHM Parameters

Whereas K_T and K_N are concentrated at zero on the individual subject datasets and are less affected by the registration process, the alignment of K_B distributions is significantly improved (see Fig. 3). GHM fits on the registered hearts produce a K_B distribution that is more consistent across all subjects. This also supports the quality of the registration process since no fiber orientation information was used in its computation, and suggests a strong correlation between fiber orientation and myocardial shape.

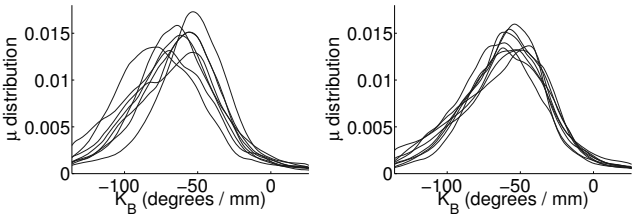

(a) $\mu(K_B)$ before registration (b) $\mu(K_B)$ after registration

Fig. 3. Effect of registration and shape normalization on K_B. (a) Computing the GHM parameters on the original hearts produces unaligned K_B distributions. (b) The groupwise registration process yields aligned K_B distributions.

3.2 Statistics on GHM Parameters

Statistics on the GHM are computed by considering the mean and standard deviation of $K_{T,N,B}$ across equivalent points in all hearts within a species. Fig. 4 show the mean K_B and standard deviation, as well as the error of fit of the GHM, for the rat and canine datasets. These results are summarized in Table 1. The low error of fit and stability of the K_B parameter for both datasets show that the GHM is an effective descriptor of fiber bundle variability. The analysis of the rat dataset is currently limited by a coarse imaging resolution when compared with the canine study. This may also explain the greater variability observed in rats. Inter-species discrepancies may also be attributed to their myocardial thickness difference, anagolously to the way registration compensates for intra-species variability.

As a first approximation, the average myocardial thickness can be used to factor out this difference in myocardial thickness which is on average 4.1 times thicker in dogs (10.3 mm) than in rats (2.5 mm). Multiplying the K_B distributions by this factor makes both species overlap.

Table 1. Per-voxel mean, standard deviation, and error of the GHM parameter fits

	K_T (°/mm)	K_N (°/mm)	K_B (°/mm)	fitting error (°)
Rat	$-1° \pm 8°$	$-2° \pm 8°$	$-63° \pm 19°$	$6.5° \pm 2.5°$
Dog	$0° \pm 8°$	$-1° \pm 6°$	$-13° \pm 10°$	$6.0° \pm 3.0°$

3.3 Transmural GHM Parameters

The variability of the GHM can be assessed in the direction from the epicardium to endocardium, a strategy commonly used for studying the trans-myocardial course of the helix angle [9]. An outer wall envelope was computed using the distance transform of the average heart. From this envelope, normals were tracked throughout the myocardium depth. Fig. 5 shows the transmural distribution of the GHM parameters, with the mode of each transmural depth connected in blue. These distributions are in agreement with the reported values of Table 1. They show a concentration of the curvature parameters K_T and K_N around $0°$/mm along with low fitting errors across the myocardium. The distribution of K_B is centered around $-10°$/mm for the dog and of $-60°$/mm for the rat. The transmural variation of K_B indicates a deceleration near the epicardium followed by a steady region and then deceleration towards the endocardium. This behavior may be related to the circular patterns seen in 4(d) which indicate a sudden change in the average K_B. These patterns suggest a salient second-order fiber bundle organization in the cardiac wall. However, the manner in which transmural penetration lines were sampled does not consider the positional variation of this organization. As a result the differential structure observed is blurred across different myocardial depths.

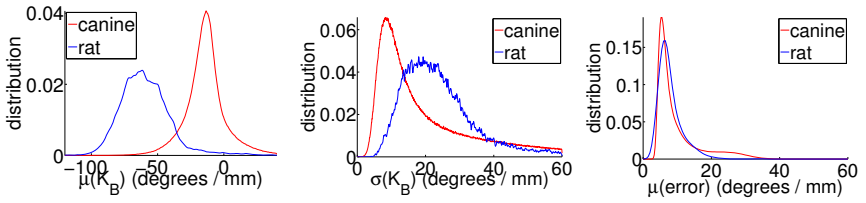

(a) $\mu(K_B)$ (b) $\sigma(K_B)$ (c) $\mu(\text{error})$

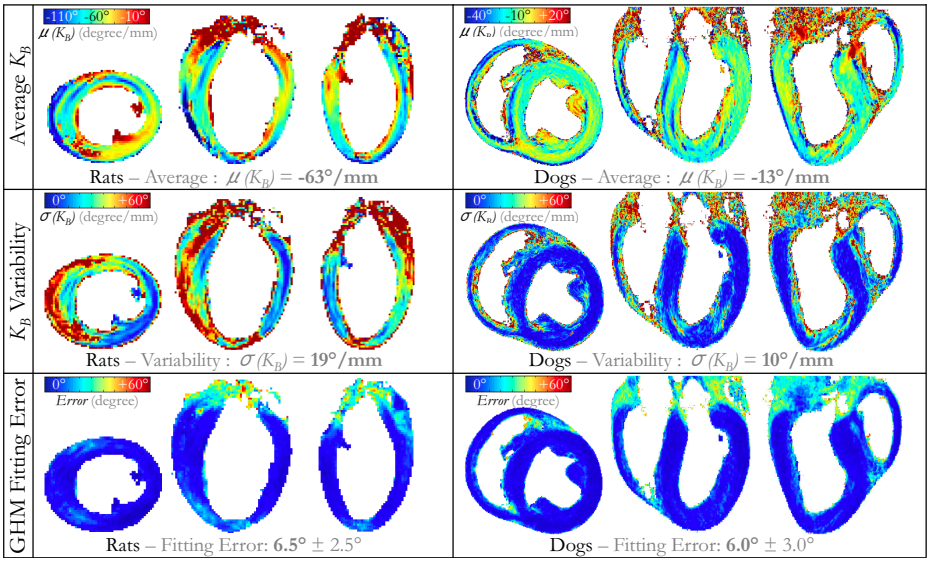

(d) Spatial distribution of the average and standard deviation of K_B, and fitting error.

Fig. 4. GHM atlas showing the parameter K_B and error of fit for the rat and canine datasets. (a) The average K_B and (b) the voxel-wise standard deviation has a distribution mode of $K_B = -63(\pm 19)^\circ/mm$ for rats and $K_B = -13(\pm 10)^\circ/mm$ for dogs. (c) The error of fit is $6.5(\pm 2.5)^\circ$ for rats and $6.0(\pm 3)^\circ$ for dogs. (d) K_B spatial variability in the lateral part of the left ventricle for the rat dataset is larger due to a challenging voxel-wise registration caused by collapsed right ventricles. The thinner myocardium of the rat compared to the dog combined with a similar turning of the helix angle yields larger GHM curvature parameters and also causes a greater voxel-wise variability. Overall, the spatial distributions indicate low errors of fit across both the rat and canine population.

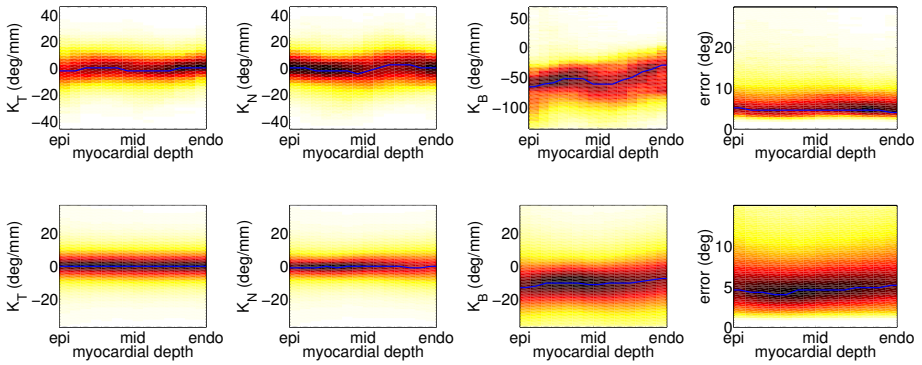

Fig. 5. Transmural distribution (y axis) of the GHM parameters K_T, K_N, K_B and fitting error as a function of transmural depth (x axis) from epicardium to endocardium for the rat (top) and canine (bottom). The coloring shows the probability distribution of a GHM parameter at a particular transmural depth, and blue lines join the distribution modes along the transmural depth.

4 Conclusion

This article presents a framework for characterizing the differential geometry of myocardial fibers in a population by registering them to an atlas, moving beyond considerations of individual fibers. Our results support a previous study on individual hearts [12], which found $K_{T,N}$ centered at $0°/\text{mm}$ and a stable negative K_B, and indicate stability in all curvature parameters across corresponding intra-species myocardial locations, particularly in the lateral portion of the left ventricle. Combined with a lower fitting error due to the effect of registering the hearts to the atlas and using an improved fitting method, these results corroborate the view that K_B is a salient descriptor of fiber bundle variability. Transmural sampling further supports this observation and indicates a stable organization of fiber bundles throughout the myocardium. However, it remains challenging to distinguish the true variability of fiber bundles from errors due to acquisition and registration. In particular, the rat dataset may be affected by partial volume effects, coarse imaging resolution, and right ventricle collapse. Future work includes the study of inter-species GHM parameter correspondences and the effect of myocardiopathies on the organization of fiber bundles. In addition, circular patterns seen in the GHM K_B volumes hint towards a specific fiber bundle organization in the cardiac wall, which remains to be studied. With ongoing research in *in vivo* imaging [18], our framework could pave the way for personalized cardiac modeling based on the differential structure of myofibers in the heart wall.

References

1. Streeter, D., Spotnitz, H., Patel, D., Ross, J., Sonnenblick, E.: Fiber orientation in the canine left ventricle during diastole and systole. Circ. Research 24(3) (1969)
2. Hooks, D.A., Tomlinson, K.A., Marsden, S.G., LeGrice, I.J., Smaill, B.H., Pullan, A.J., Hunter, P.J.: Cardiac microstructure: implications for electrical propagation and defibrillation in the heart. Circ. Research 91(4) (2002)
3. Greenbaum, R.A., Ho, S.Y., Gibson, D.G., Becker, A.E., Anderson, R.H.: Left ventricular fibre architecture in man. British Heart Journal 45(3) (1981)
4. Basser, P.J., Mattiello, J., LeBihan, D.: MR diffusion tensor spectroscopy and imaging. Biophysical Journal 66(1) (1994)
5. Hsu, E.W., Henriquez, C.S.: Myocardial fiber orientation mapping using reduced encoding diffusion tensor imaging. CMR 3(4) (2001)
6. Helm, P.A., Tseng, H.J.J., Younes, L., McVeigh, E.R., Winslow, R.L.: Ex vivo 3D diffusion tensor imaging and quantification of cardiac laminar structure. MRM 54(4) (2005)
7. Rohmer, D., Sitek, A., Gullberg, G.T.: Reconstruction and visualization of fiber and laminar structure in the normal human heart from ex vivo diffusion tensor magnetic resonance imaging (DTMRI) data. Invest. Radiol. 42(11) (2007)
8. Sundar, H., Shen, D., Biros, G., Litt, H., Davatzikos, C.: Estimating myocardial fiber orientations by template warping. In: ISBI (2006)
9. Lombaert, H., Peyrat, J.-M., Croisille, P., Rapacchi, S., Fanton, L., Cheriet, F., Clarysse, P., Magnin, I., Delingette, H., Ayache, N.: Human atlas of the cardiac fiber architecture: Study on a healthy population. TMI 31(7) (2012)
10. Peyrat, J.-M., Sermesant, M., Pennec, X., Delingette, H., Xu, C., McVeigh, E.R., Ayache, N.: A computational framework for the statistical analysis of cardiac diffusion tensors: application to a small database of canine hearts. TMI 26(11) (2007)
11. Bronzino, J.D.: Biomedical Engineering Handbook, vol. 1. Springer (1995)
12. Savadjiev, P., Strijkers, G.J., Bakermans, A.J., Piuze, E., Zucker, S.W., Siddiqi, K.: Heart wall myofibers are arranged in minimal surfaces to optimize organ function. Proc. Natl. Acad. Sci. USA. 109(24) (2012)
13. Piuze, E., Sporring, J., Siddiqi, K.: Moving frames for heart fiber geometry. In: Information Processing in Medical Imaging (2013)
14. Piuze, E., Kry, P., Siddiqi, K.: Generalized helicoids for modeling hair geometry. Computer Graphics Forum 30(2) (2011)
15. Lombaert, H., Grady, L., Pennec, X., Peyrat, J.-M., Ayache, N., Cheriet, F.: Groupwise spectral Log-Demons framework for atlas construction. In: MCV MICCAI (2012)
16. Geerts, L., Bovendeerd, P., Nicolay, K., Arts, T.: Characterization of the normal cardiac myofiber field in goat measured with mr-diffusion tensor imaging. AJP: Heart and Circ. Physiol. 283 (2002)
17. Lombaert, H., Peyrat, J.-M., Fanton, L., Cheriet, F., Delingette, H., Ayache, N., Clarysse, P., Magnin, I., Croisille, P.: Statistical atlas of human cardiac fibers: Comparison with abnormal hearts. In: Camara, O., Konukoglu, E., Pop, M., Rhode, K., Sermesant, M., Young, A. (eds.) STACOM 2011. LNCS, vol. 7085, pp. 207–213. Springer, Heidelberg (2012)
18. Toussaint, N., Stoeck, C.T., Sermesant, M., Schaeffter, T., Kozerke, S., Batchelor, P.G. In: vivo human cardiac fibre architecture estimation using shape-based diffusion tensor processing. Medical Image Analysis (2013)